International Journal of Modern Physics B
Vol. 27, No. 6 (2013) 1350018 (26 pages)
© World Scientific Publishing Company
DOI: 10.1142/S0217979213500185

World Scientific
www.worldscientific.com

NONCOLLINEAR MAGNETIC ORDER IN THE DOUBLE PEROVSKITES: DOUBLE EXCHANGE ON A GEOMETRICALLY FRUSTRATED LATTICE

RAJARSHI TIWARI* and PINAKI MAJUMDAR†
Harish-Chandra Research Institute, Chhatnag Road, Jhusi, Allahabad 211019, India
**rajarshi@hri.res.in*
†*pinaki@hri.res.in*

Received 9 September 2012
Revised 9 December 2012
Accepted 10 December 2012
Published 30 January 2013

Double perovskites (DPs) of the form $A_2BB'O_6$ usually involve a transition metal ion, B, with a large magnetic moment, and a nonmagnetic ion B′. While many DPs are ferromagnetic, studies on the underlying model reveal the possibility of antiferromagnetic (AF) phases as well *driven by electron delocalization.* In this paper we present a comprehensive study of the magnetic ground state and T_c scales of the minimal DP model in three dimensions using a combination of spin-fermion Monte Carlo and variational calculations. The effective magnetic lattice in three dimensions is face centered cubic (FCC) and so geometrically frustrated. This promotes noncollinear spiral states and "flux" like phases in addition to collinear AF order. We map out the possible magnetic phases for varying electron density, "level separation" $\epsilon_B - \epsilon_{B'}$, and the crucial B′B′ (next neighbour) hopping t'.

Keywords: Double perovskite; double exchange; geometric frustration; noncollinear magnetism.

1. Introduction

Double perovskites (DPs) constitute a large family of materials[1,2] with molecular formula $A_2BB'O_6$, where A is an alkali or alkaline earth metal, and B and B′ are typically transition metals. Although DPs have been studied for decades,[3] the discovery of high T_c ferromagnetism and half-metallicity in Sr_2FeMoO_6 has led to renewed interest in their properties. Later, in a number of explorations it was discovered that these materials are candidates for various technological applications, e.g., in spintronics[4] (Sr_2FeMoO_6), magneto-dielectrics[5,6] (La_2NiMnO_6), and magneto-optics[7] (Sr_2CrOsO_6,Sr_2CrReO_6). Their properties are determined by the couplings on the B and B′ ions, the B and B′ valence state, and the structural order in the B–B′ lattice.

The magnetism in the DP's arises from a combination of (i) Hund's coupling on the B, B′ ions and (ii) electron delocalization. While there are important DP's where both B and B′ are magnetic ions, in the current work we will restrict ourselves to materials where only one ion, B, say, is magnetic. For example, in Sr_2FeMoO_6 (SFMO) the B atom (Fe) is magnetic while B′ (Mo) is nonmagnetic.[8] Even in this restricted class, a large variety of compounds can be realized by taking $3d$, $4d$ or $5d$ transition metals as B and B′, and alkaline earths or rare-earths as A. These lead to a variety of properties, e.g., high T_c ferro(or ferri) magnetism (FM), with half-metallic[9,10] or insulating[11] behavior.

There have been several attempts at a theoretical understanding of the magnetism in these materials. These consist of (i) *ab initio* electronic structure calculations, and (ii) model Hamiltonian based approaches. The *ab initio* calculations[6–8] provide material specific information about the electronic structure and allow a rough estimate[12] of the T_c. Unfortunately, these calculations are rather complicated for noncollinear magnetic phases that are likely in a frustrated magnetic lattice, see Fig. 1 (we discuss the frustration aspect in detail later). In such situations model Hamiltonian studies can provide some insight on possible ordered states.

Early model calculations for DP's used dynamical mean field theory (DMFT) to estimate T_c and the magnetic stability window,[13,14] focusing on FM. Earlier work on the classical Kondo lattice[15–18] had revealed that variation in carrier density can lead to a wide variety of phases in a spin-fermion problem. Indeed, calculation[19] in a two dimensional (2D) model of DP's confirmed the existence of AF metallic, albeit collinear, phases. *Ab initio* calculations have confirmed the possibility of *collinear* AF metallic phases in realistic three dimensional (3D) situations.[20] The

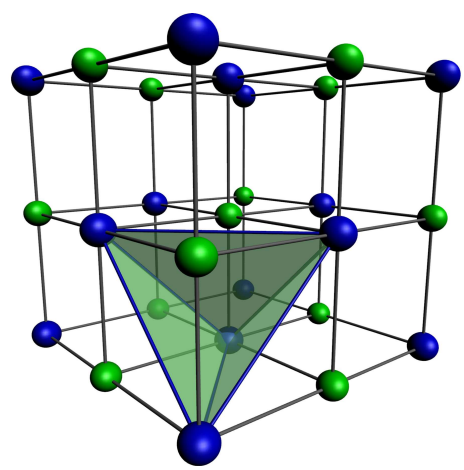

Fig. 1. (Color online) The structure of B–B′ lattice in an ordered DP. The B and B′ alternate (as in rock-salt) in the ordered structure. If the bottom corner (blue) atom is B, then its B nearest neighbors (connected by blue lines) are also nearest neighbors of each other. The triangles preclude a "G-type" AF phase.

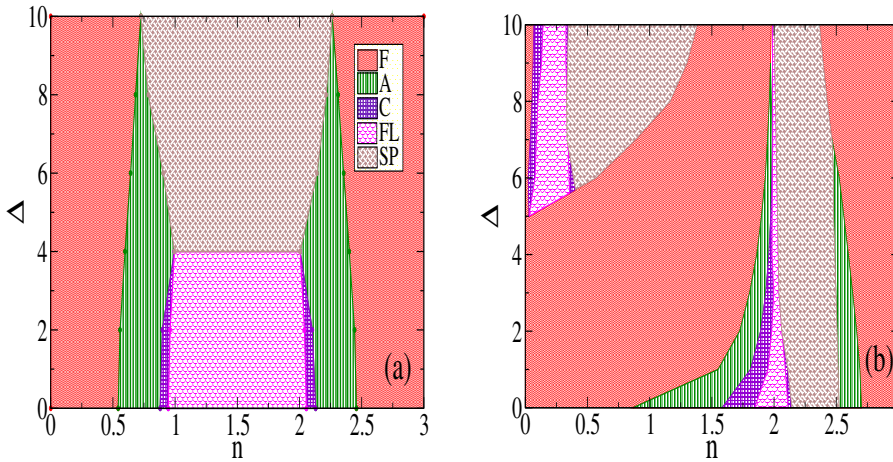

Fig. 2. (Color online) Magnetic ground state for varying electron density, n, and effective B–B′ level separation, Δ. Left: phase diagram with only BB′, i.e., nearest neighbour, hopping. Right: phase diagram when an additional B′B′ hopping, $t'/t = -0.3$, is included. The labels are: F (ferromagnet), A (planar phase), C (line like), FL ("flux") and SP (spiral). This figure does not show the narrow windows of phase separation (PS) in the model. The phase diagrams are generated via a combination of MC and variational calculations on lattices of size upto $20 \times 20 \times 20$.

"frustrated" character of the 3D DP lattice raises the intriguing possibility of doping driven noncollinear magnetic phases as well. Our study aims to explore this issue in detail.

Our main results are the following. Using a combination of Monte Carlo (MC) and variational minimization, we map out the magnetic ground state (Fig. 2) at large Hund's coupling for varying electron density and B–B′ level separation. In addition to FM, and collinear A- and C-type order, the phase diagram includes large regions of noncollinear "flux" and spiral phases and windows of PS. Modest B′B′ hopping leads to significant shift in the phase boundaries, and "particle-hole asymmetry". We provide estimates of the T_c of these nontrivial magnetic phases.

The paper is organized as follows. In Sec. 2 we describe the model and methods, Sec. 3 describes our results in the particle-hole symmetric case ($t' = 0$), and Sec. 4 describes the effect of finite t'. Section 5 discusses some issues of modeling the real DP. Section 6 concludes the paper.

2. Model and Method

Previous study of DPs in two dimensions[19] revealed three collinear phases, namely FM, a diagonal stripe phase (FM lines coupled antiferromagnetically) and a "G-type" phase (up spin surrounded by down and vice versa). In 2D the B sub-lattice is square and bipartite, so there is no frustration. In a 3D *simple cubic* B lattice the counterparts of the 2D phases would be FM, A-type (planar), C-type (line like) and G-type. The magnetic B ion lattice in the DP's is, however, FCC which is

nonbipartite, so while one can construct FM and planar A-type phases, the C-type phase is modified and the G-type phase cannot exist.

Figure 1 briefly indicates why it is impossible to have an "up" (↑) B ion to be surrounded by only "down" (↓) B ions, i.e., the G-type arrangement. Two B neighbors of a B ion are also neighbors of each other, frustrating G-type order. The suppression of the G-type phase, which occupies a wide window in 2D, requires us to move beyond collinear phases in constructing the phase diagram for 3D. We will discuss the variational family in Sec. 2.3.

2.1. *Model*

The alternating arrangement of B and B′ ions in the ordered cubic DPs is shown in Fig. 1. We use the following one band model on that structure:

$$H = \epsilon_B \sum_{i\in B} f^\dagger_{i\sigma} f_{i\sigma} + \epsilon_{B'} \sum_{i\in B'} m^\dagger_{i\sigma} m_{i\sigma} - \mu\hat{N} - t\sum_{\langle ij\rangle} f^\dagger_{i\sigma} m_{j\sigma} + J\sum_{i\in B} \mathbf{S}_i \cdot f^\dagger_{i\alpha}\boldsymbol{\sigma}_{\alpha\beta} f_{i\beta}\,. \quad (1)$$

The $f^\dagger$ corresponds to the B ions and the $m^\dagger$ to the B′. ϵ_B and $\epsilon_{B'}$ are "onsite" energy on the B and B′ sites, respectively, e.g., the t_{2g} level energy of Fe and Mo in SFMO. μ is the chemical potential and $\hat{N} = \sum_{i\sigma}(f^\dagger_{i\sigma} f_{i\sigma} + m^\dagger_{i\sigma} m_{i\sigma})$ is the total electron number operator. t is the hopping amplitude between nearest neighbor B and B′ ions. We augment this model later to study first neighbor B′B′ hopping t' as well. J is the (Hund's) coupling between the B core spin and the f conduction electron. We will use $|\mathbf{S}_i| = 1$, and absorb the magnitude of $\mathbf{S}$ in J. $\sigma^\mu_{\alpha\beta}$ are the Pauli matrices.

The model has parameters J, ϵ_B, $\epsilon_{B'}$ and μ (or n). Since only the level difference matters, we set $\epsilon_{B'} = 0$. We have set $t = 1$, and use $J/t \gg 1$ so that the conduction electron spin at the B site is slaved to the core spin orientation. However, to keep the *effective* level difference between B and B′ sites finite we use the parameter $\Delta = \epsilon_B - J/2$, and explore the phases as a function of n and Δ/t. We will present results for $t'/t = 0$ and ± 0.3.

A schematic for the levels is shown in Fig. 3. The structural unit cell of the system has two (one B, one B′) atoms, which amounts to four atomic levels (two up spin, two down spin). The two spin levels at the B site are separated by JS and overlap with two spin degenerate levels of the B′ site at $\epsilon_{B'} = 0$. We take the large J limit, and take $\epsilon_B = J/2 + \Delta$ with Δ in the range (0–10). One B band become centered at Δ and second goes to JS + Δ. In this situation the down spin B and two B′ bands overlap while up spin B band is always empty. The relevant electron density window includes the lowest three bands, so our electron density will be in the range $[0, 3]$.

To get a general feel of the band structure of the particle hole symmetric case, we notice that we have three levels (excluding the highest $f_\uparrow$ level at JS + Δ which

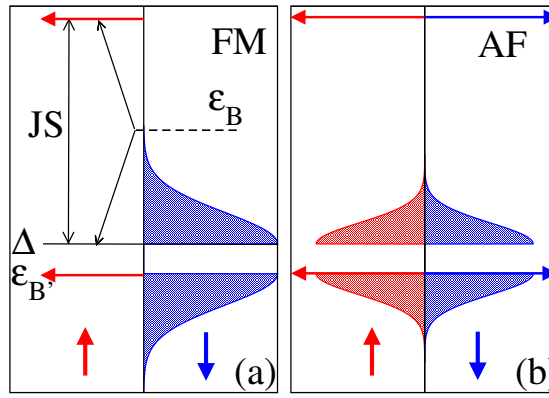

Fig. 3. (Color online) Level scheme and schematic band structure for the DP model when only B–B′ hopping is allowed. The arrows denote localized atomic levels. Red and blue denote ↑ and ↓ spins respectively. The atomic level scheme is shown in (a). where the spin degenerate B′ levels are at $\epsilon_{B'} = 0$ and the spin split B levels are at $\epsilon_B \pm \mathrm{JS}/2$. We define the effective B level as $\Delta = \epsilon_B - \mathrm{JS}/2$. When $\mathrm{JS} \gg t$, the levels at $\epsilon_{B'}$ and Δ hybridize to create bands, shown for the FM case in (a), and for a collinear AF phase in (b).

remains empty and is redundant for our purpose) in atomic limit. These include one spin slaved $f_\downarrow$ level at Δ, and the two $m_\uparrow$, $m_\downarrow$, levels which overlap with the $f_\downarrow$ levels depending on the spin configurations. This overlap leads to electron delocalization and band formation.

In the ferromagnetic case, Fig. 3(a), only one spin channel (say $m_\downarrow$) gets to delocalize through f sites and forms two bands, separated by a band gap of Δ, while other spin channel (say $m_\uparrow$) is localized at 0.

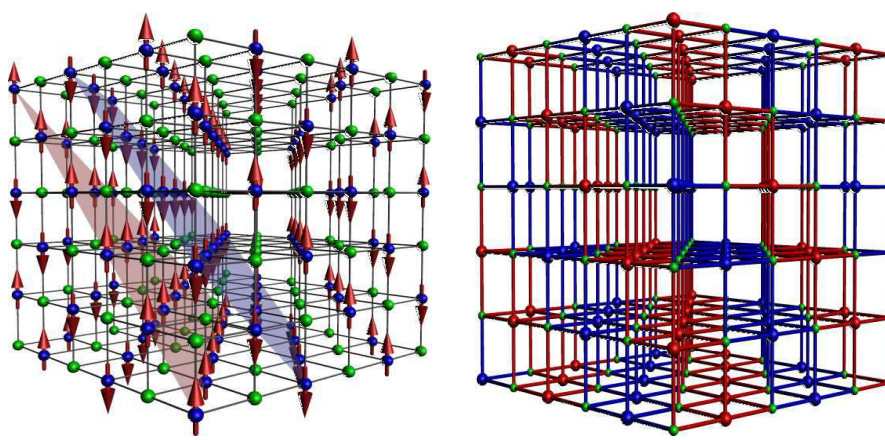

Fig. 4. (Color online) Left: Spin configuration for "A-type" order. The spins are parallel within the 111 planes (shown) and are anti-parallel between neighboring planes. Right: The differently colored bands show the electron delocalization pathway for up and down spin electrons in the A-type phase. The delocalization is effectively 2D.

For collinear AF configurations, the rough band scheme is as shown in Fig. 3(b). The conduction path gets divided into two sub-lattices, such that each spin channel gets to delocalize in one sub-lattice (in which all the core spins point in same direction, making the sub-lattice ferromagnetic.) See Figs. 4 and 5 for the details of the conduction path. In one such sub-lattice, only one of the $\uparrow$ or $\downarrow$ is delocalized, the other remains localized. The roles of $\uparrow$ and $\downarrow$ are reversed in going from one sub-lattice to other, as a result one gets spin-degenerate localized and dispersive bands for AF phases.

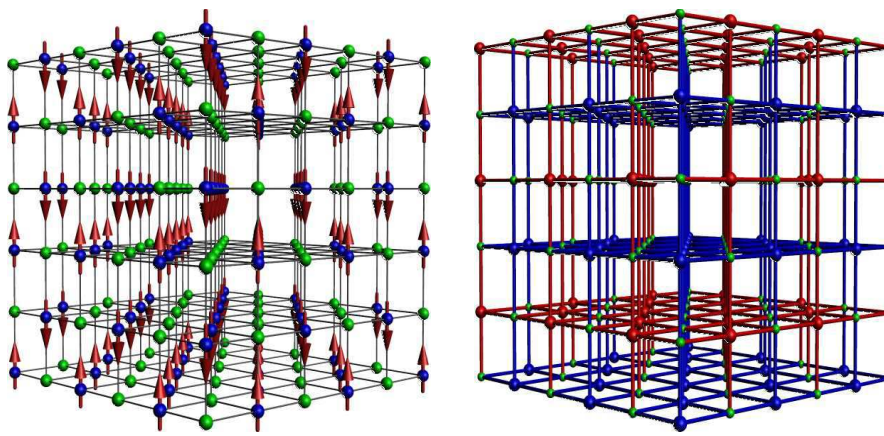

Fig. 5. (Color online) Left: Spin configuration in the "C-type" phase. Core spins are parallel on alternating 110 planes, and anti-parallel on neighboring planes. Right: the delocalization path, consisting of the 110 planes and the horizontal 001 planes.

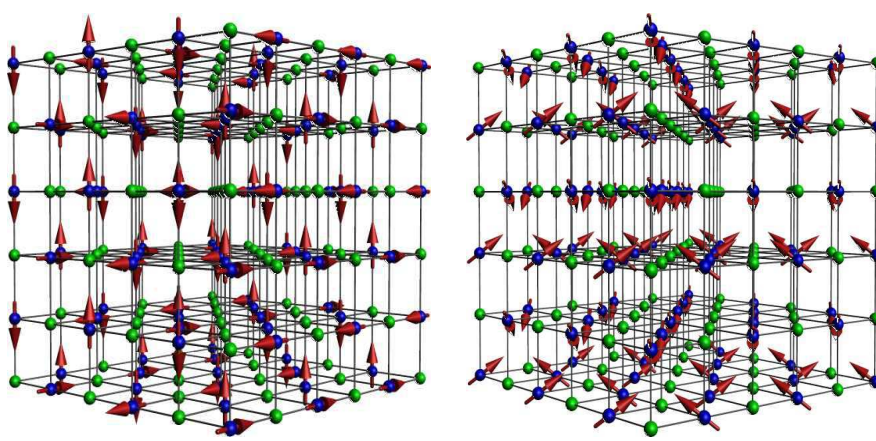

Fig. 6. (Color online) Spin configuration for a typical spiral phase (left) and the "flux" phase (right). Since the spin configurations are noncollinear the electrons delocalize over the whole system.

2.2. *Monte Carlo method*

The model involves spins and fermions, and if the spins are "large", $2S \gg 1$, they can be approximated as classical. This should be reasonable in materials like SFMO where $S = 5/2$. Even in the classical limit these spins are annealed variables and their ground state or thermal fluctuations have to be accessed via iterative diagonalization of the electronic Hamiltonian. We use a "traveling cluster" Monte Carlo (MC) method where the cost of a spin update is estimated via a small cluster Hamiltonian instead of diagonalizing the whole system.[21]

We typically use a $12 \times 12 \times 12$ system with the energy cost of a move estimated via a 4^3 cluster built around the reference site. We principally track the magnetic structure factor

$$S(\mathbf{q}) = \frac{1}{N^2} \sum_{\mathbf{r},\mathbf{r}'} \langle \mathbf{S}_{\mathbf{r}} \cdot \mathbf{S}_{\mathbf{r}'} \rangle e^{i\mathbf{q}\cdot(\mathbf{r}-\mathbf{r}')} \,, \tag{2}$$

where $\langle \cdots \rangle$ denote thermal average.

Although the magnetic lattice is FCC, the electrons delocalize on the combined B–B′ system which is a cubic lattice. Hence we define our wave-numbers $\mathbf{q}$ with respect to the full B–B′ lattice. As a result even a simple state like the ferromagnet corresponds to peaks at $\mathbf{q} = (0, 0, 0)$ and $\mathbf{q} = (\pi, \pi, \pi)$ and not just $\mathbf{q} = (0, 0, 0)$. This is because the spin field is also defined on B′ sites and it has to have zeros on these sites.

This complication, and the possibility of spiral phases, etc, mean that (i) there are multiple $\mathbf{q}$ values which could be significant at low temperature, and (ii) the $S(\mathbf{q})$ peaks could be small even in the ordered state. Combined with the intrinsic noise in MC data (which is enhanced due to a complex energy landscape, discussed later) it is sometimes difficult to identify complicated ordered phases. Therefore, to complement the MC results we have also used the following variational scheme.

2.3. *Variational scheme*

We explore a set of magnetic states, comparing their energy to locate the minimum within that family for a fixed set of electronic parameters. We use:

$$\mathbf{S}_{\mathbf{r}} = p_{\mathbf{r}}(\hat{x} \sin\theta_{\mathbf{r}} \cos\phi_{\mathbf{r}} + \hat{y} \sin\theta_{\mathbf{r}} \sin\phi_{\mathbf{r}} + \hat{z} \cos\theta_{\mathbf{r}}) \,, \tag{3}$$

where $\theta_{\mathbf{r}} = \mathbf{q}_\theta \cdot \mathbf{r}$ and $\phi_{\mathbf{r}} = \mathbf{q}_\phi \cdot \mathbf{r}$ with $p_{\mathbf{r}} = 1$ if $\mathbf{r} \in B$ and $p_{\mathbf{r}} = 0$ if $\mathbf{r} \in B'$. $\hat{x}$, etc, are unit vectors in the corresponding directions.

The vector field $\mathbf{S}_{\mathbf{r}}$ is characterized by the two wave-vectors $\mathbf{q}_\theta$ and $\mathbf{q}_\phi$. For a periodic configuration, these should be $\mathbf{q}_\theta = (2\pi/L)(q_1, q_2, q_3)$ and $\mathbf{q}_\phi = (2\pi/L)(p_1, p_2, p_3)$, where q_i's and p_i's are integers, each of which take L values in $\{0, 1, 2, 3, \ldots, L-1\}$. There are $\sim L^6$ ordered magnetic configurations possible, within this family, on a simple cubic lattice of linear dimension L.

The use of symmetries, e.g., permuting components of q_θ, etc, reduces the number of candidates somewhat, but they still scale as $\sim L^6$. For a general combination

of $\mathbf{q}_\theta, \mathbf{q}_\phi$ the eigenvalues of H cannot be analytically obtained because of the non trivial mixing of electronic momentum states. We have to resort to a real space diagonalization. The Hamiltonian matrix size is $2N$ $(= 2L^3)$ and the diagonalization cost is $\sim N^3$. So, a comparison of energies based on real space diagonalization costs $\sim N^5$, possible only for $L \leq 8$.

We have adopted two strategies: (i) we have pushed this "$\mathbf{q}_\theta, \mathbf{q}_\phi$" scheme to large sizes via a selection scheme described below, and (ii) for a few collinear configurations, where Fourier transformation leads to a small matrix, we have compared energies on sizes $\sim 400^3$.

First, scheme (i). For $L = 8$ we compare the energies of all possible phases, to locate the optimal pair $\{\mathbf{q}_\theta, \mathbf{q}_\phi\}_{\min}$ for each μ. We then consider a larger system with a set of states in the neighborhood of $\{\mathbf{q}_\theta, \mathbf{q}_\phi\}_{\min}$. If we consider $\pm\pi/L$ variation about each component of $\mathbf{q}_{\theta,\min}$, etc, that involves 3^6 states. The shortcoming of this method is that it explores only a restricted neighborhood, dictated by the small size result. We have used $L = 12, 16, 20$ within this scheme.

The phases that emerge as a result of the above process are (i) Ferromagnet (FM), (ii) A-type, (iii) C-type, (iv) "flux", and (v) three spirals SP_1, SP_2, SP_3. A-type consists of $(1, 1, 1)$ FM planes with alternate planes having opposite spin orientation (see Fig. 4 left panel). If we convert each of these planes to alternating FM lines, so that the overall spin texture is alternating FM *lines* in all directions, we get C-type phase (see Fig. 5).

The "flux" phase is different from the spiral families described using period vectors $\mathbf{q}_\theta$, $\mathbf{q}_\phi$. It is the augmented version of "flux" phase used in cubic lattice

Table 1. Candidate phases, the associated $\mathbf{q}_\theta$, $\mathbf{q}_\phi$, for the spirals, and the peak locations in the structure factor $S(\mathbf{q})$. All the $\mathbf{q}$ components have the same saturation value, given by $1/2N_p$, where N_p is the number of nonzero $\mathbf{q}$ peaks in the $S(\mathbf{q})$. $N_p = 2$ for FM, A and C, $N_p = 4$ for $\uparrow\uparrow\downarrow\downarrow$ and SP_1, $N_p = 6$ for flux and $N_p = 8$ for SP_2 and SP_3. The factor of $1/2$ comes as we have half the spins at zero value, which halves the normalization.

Phase	Peak location in $S(\mathbf{q})$
FM	$(0,0,0)$, (π,π,π)
A-type	$\left(\frac{\pi}{2},\frac{\pi}{2},\frac{\pi}{2}\right)$, $\left(\frac{3\pi}{2},\frac{3\pi}{2},\frac{3\pi}{2}\right)$
C-type	$(0,0,\pi)$, $(\pi,\pi,0)$
Flux	$(\pi,0,0)$, $(0,\pi,0)$, $(0,0,\pi)$
	$(\pi,\pi,0)$, $(\pi,0,\pi)$, $(0,\pi,\pi)$
$\uparrow\uparrow\downarrow\downarrow$ phase	$\left(\frac{\pi}{2},0,0\right)$, $\left(\frac{3\pi}{2},0,0\right)$, $\left(\frac{\pi}{2},\pi,\pi\right)$, $\left(\frac{3\pi}{2},\pi,\pi\right)$
SP_1: $\mathbf{q}_\theta = \left(0,\frac{\pi}{2},\pi\right)$, $\mathbf{q}_\phi = 0$	$\left(0,\frac{\pi}{2},\pi\right)$, $\left(\pi,\frac{\pi}{2},0\right)$, $\left(0,\frac{3\pi}{2},\pi\right)$, $\left(\pi,\frac{3\pi}{2},0\right)$
SP_2: $\mathbf{q}_\theta = \left(0,\frac{\pi}{2},\pi\right)$	$\left(0,\frac{\pi}{2},\pi\right)$, $\left(\pi,\frac{\pi}{2},0\right)$, $\left(0,\frac{3\pi}{2},\pi\right)$, $\left(\pi,\frac{3\pi}{2},0\right)$
$\mathbf{q}_\phi = \left(0,\frac{\pi}{2},0\right)$	$(0,0,\pi)$, $(\pi,0,0) + (\pi,\pi,0) + (0,\pi,\pi)$
SP_3: $\mathbf{q}_\theta = \left(0,\frac{\pi}{2},\pi\right)$	$\left(0,\frac{\pi}{2},\pi\right)$, $\left(\pi,\frac{\pi}{2},0\right)$, $\left(0,\frac{3\pi}{2},\pi\right)$, $\left(\pi,\frac{3\pi}{2},0\right)$
$\mathbf{q}_\phi = \left(\frac{\pi}{2},0,\frac{\pi}{2}\right)$	$\left(\frac{\pi}{2},\frac{\pi}{2},\frac{3\pi}{2}\right)$, $\left(\frac{3\pi}{2},\frac{3\pi}{2},\frac{\pi}{2}\right)$, $\left(\frac{\pi}{2},\frac{3\pi}{2},\frac{3\pi}{2}\right)$, $\left(\frac{3\pi}{2},\frac{\pi}{2},\frac{\pi}{2}\right)$

double exchange model by Alonso *et al.* (Table 1 of Ref. 17). It has spin-ice like structure, and is described by:

$$\mathbf{S}(\mathbf{r}) = \frac{p(\mathbf{r})}{\sqrt{3}}((-1)^{y+z}, (-1)^{z+x}, (-1)^{x+y})$$

The spiral SP_n phases are characterized by commensurate values of $\mathbf{q}_\theta, \mathbf{q}_\phi$ (See Table 1 for details of periods and the S($\mathbf{q}$) peaks).

The simplest, SP_1 can be viewed as $\pi/2$-angle pitch in the (110), (101) and (011) directions. The other two spirals SP_2, SP_3 are respectively C-type and A-type modulations upon SP_1. Just as flipping alternate $1, 1, 1$ planes in a FM leads to the A-type phase, flipping the spins in the (111) planes alternatively in SP_1, leads to SP_3. Analogously, flipping FM lines in a FM and leads to C-type order and a similar exercise on SP_1 leads to SP_2. This modulation is also seen in the $S(\mathbf{q})$ peaks of SP_2 and SP_3. See the Table 1, where all the three spirals have four $S(\mathbf{q})$ peaks common, and SP_2 and SP_3 possess extra $S(\mathbf{q})$ peaks of the A-type and C-type correlations.

In scheme (ii) we take collinear phases from the phase diagram via MC and variational scheme (i), and compare them on very large lattices. This does not require real space diagonalization. The simple periodicity of these phases leads to coupling between only a few $|\mathbf{k}\rangle$ states. The resulting small matrix can be diagonalized for the eigenvalues and these summed numerically. We also did it for the "flux" phase, where the resulting matrix is a bit larger, but still it gets us access to eigenvalues for the "flux" phase on large lattices. The details of this calculation, and the the magnetic phase diagram from comparison of FM, A, C and flux phases at large lattice size are discussed in Appendix A. Where the collinear phases (and "flux") seem to dominate the phase diagram we compute phase boundaries by calculating the energy on very large lattices.

3. Results: Particle-Hole Symmetric Case

The electrons move on the cubic lattice divided into two FCC sub-lattices each of which accommodate B and B′ sites. For each of these sub-lattice, one can define particle-hole transformation[22] for B and B′ sub-lattices as $f_i \to f_i^\dagger$ and $m_{i\sigma} \to -m_{i\sigma}^\dagger$. This transforms the Hamiltonian as $H_{\text{particle}}(\Delta, t, t') - \mu N \to H_{\text{hole}}(-\Delta, t, -t') - (\mu - \Delta)N$. When $t' = 0$, this simplifies to $H(\Delta, t) - \mu N \to H(-\Delta, t) - (\mu - \Delta)N$ which reflects in the phase diagram as the repetition of the phases after half-filling. Introducing the t' hopping destroys this symmetry, but a reduced symmetry still remains relating $(\Delta, t, t') \to (-\Delta, t, -t')$, which is reflected in the phase diagrams of particle-hole asymmetric case.

We first discuss the case of particle-hole symmetry, i.e., $t' = 0$, and the case of $t' \neq 0$ in the next section. For each of these cases we first discuss the MC results since these are unbiased, though affected by finite size and the cluster update mechanism. This provides a feel for the relevant candidate states that we can explore more

carefully within a variational scheme. It also provides an estimate of T_c, not readily available within the variational scheme.

Following this we show the ground states and PS windows that emerge from the variational calculation for varying n and Δ/t. We also provide an alternate estimate of the "T_c" of these phases by calculating the energy difference $\delta E(n) = (E_{\rm pm}(n) - E_{\rm ord}(n))/N_s$, that the system gains via magnetic ordering. Here $E_{\rm pm}$ is the electronic energy averaged over disordered (paramagnetic) spin configurations while $E_{\rm ord}$ is the energy of the magnetically ordered ground state, both at the same electron density n. $N_s(= N/2)$ is the number of spins in the system. The phases that dominate the phase diagram are listed in Table 1, with the associated $\mathbf{q}_\theta$, $\mathbf{q}_\phi$, and the peak locations in the structure factor.

3.1. *Monte Carlo*

We studied a $N = 12^3$ system using the cluster based update scheme. We used a large but finite J to avoid explicitly projecting out any electronic states,[a] since that complicates the Hamiltonian matrix but allows only a small increase in system size. The magnetic phases were explored for $\Delta = 0, 4$ and 10. An illustrative plot of peak features in $S(\mathbf{q})$ as function of temperature T, is shown in Fig. 7 for some typical densities, where, for FM, $S(\mathbf{q}_{\rm FM})$ shows monotonic decrease of T_c with increasing Δ. For A-type and "flux" phase, the $S(\mathbf{q})$ data shows a number of sub-dominant $\mathbf{q}$ peaks whose number keeps increasing as we move to more complicated phases with increasing density.

Using the structure factor data, we establish the $n - T_c$ phase diagram for $\Delta = 0, 4, 10$ that is plotted in Fig. 8. The MC captures mainly three collinear phases, namely FM, A-type, and a $\uparrow\uparrow\downarrow\downarrow$ phase. The $\uparrow\uparrow\downarrow\downarrow$ phase corresponds to two FM up planes followed by two FM down planes and so forth. As the carrier density is increased via increasing μ, we find a FM phase followed by the A-type AF. A $\uparrow\uparrow\downarrow\downarrow$ phase appears in a thin window surrounded by FM itself. We suspected this as a finite size effect, and a comparison with the energy of the FM on larger lattices (20^3), shows that the FM is indeed the ground state in the thermodynamic limit, and so we consider FM and $\uparrow\uparrow\downarrow\downarrow$ collectively as FM only, and presence of $\uparrow\uparrow\downarrow\downarrow$ is not indicated in the phase diagram.

The FM is stable at the ends of the density window, and its region of occurrence is slowly enhanced as we increase Δ, see Fig. 2 as well. The T_c however decreases with increasing Δ since the degree of B–B$'$ mixing (and kinetic energy) decreases.

With further increase in n the 2D system is known to make a transition to a line-like phase, and then a "G-type" phase (up spin surrounded by down, etc). In 3D one would expect the FM to change to a "planar" (A-type) phase, then a "line like" (C-type) phase and finally to a G-type phase if possible. All of these are of

[a]We have worked on $\Delta \in [-10, 10]$, so J has to be large compared to it. We used $J = 1000$, as the atomic bands which, for finite J, are actually dispersive (of band-width $\sim \mathcal{O}(1/\Delta)$) become actually atomic to required numerical accuracy.

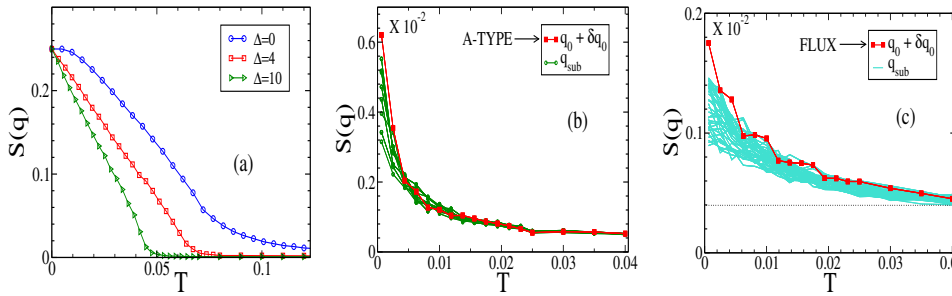

Fig. 7. (Color online) Temperature dependence of structure factor peaks for three typical densities and $t' = 0$. (a). For $\Delta = 0, 4, 10$, ferromagnetic order at $n = 0.20$. (b). The growth of A-type correlations (and the noise around the principal peak, at $n = 0.50$. The ordering wave-vector $\mathbf{q}_0$ is listed in Table 1. $\delta\mathbf{q}_0$ are $\sim \mathcal{O}(1/L)$ (c). "flux" type correlations at $n = 1.50$. The features are at and around the ordering wave-vector in Table 1. Note the scale factors on the y-axis in (b) and (c).

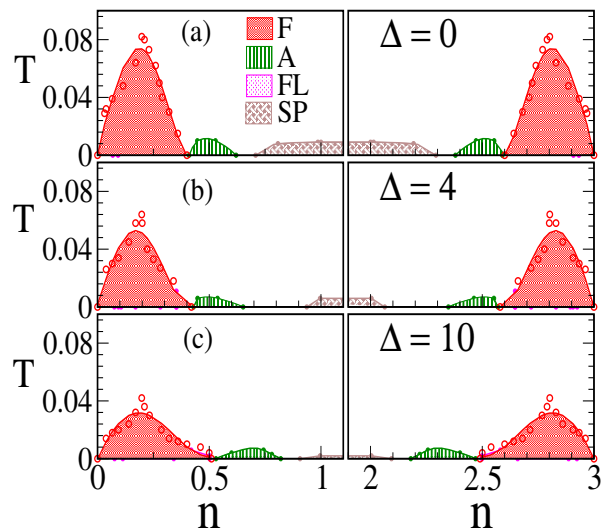

Fig. 8. (Color online) $n - T_c$ diagram for $\Delta = 0, 4, 10$ (top to bottom rows) as estimated from the MC. Starting from low density ($n = 0$) towards high density ($n = 1$), we find FM with high T_c, thin window of A-type with very low T_c as compared to FM, followed by "flux" in $\Delta = 0$ and "spiral" in larger Δ case. The symbols are the actual MC estimated T_c, while the smooth lines are fit to the data.

course collinear phases, and geometric constraints may lead to noncollinear order as well.

While we do access the A-type phase with some difficulty, our MC cannot access the long range ordered C-type phase. However, we see clear evidence of C-type correlations in the structure factor. Comparing the energy of the ideal C-type phase with the short range correlated phase that emerges from the MC we infer that such

order is indeed preferred. However, we cannot estimate a reliable T_c scale. In the next section we will see that the variational calculation confirms the stability of the C-type, among collinear phases, in this density window, and will get a rough estimate of the T_c from the energy δE.

The G-type phase is geometrically disallowed on the B sub-lattice due to its FCC structure. An examination of the structure factor in the density window $n = [1, 2]$ suggests "flux" like correlations at small Δ which evolves into a spiral at larger Δ. The frustration reduces the T_c of the phases in this density window compared to that of the FM. We studied the situation in 2D, where the system is unfrustrated, and the numbers below highlight the impact of frustration. In 2D, MC results yield $T_c^{\rm AF}/T_c^{\rm FM} \lesssim 1$, while in 3D $T_c^{\rm AF}/T_c^{\rm FM} \lesssim 0.1$. We had focused on AF states at $n \sim 1.5$. If we compare the $(\delta E)^{AF}/(\delta E)^{FM}$ for 2D and 3D, the numbers come out to be ~ 1.1 and 0.5 respectively.[b] The comparisons suggest a significant decrease in the binding energy (and hence T_c) of the AF phases relative to the FM as we move from 2D to 3D.

When $t' = 0$, the electron delocalization happens through B–B′–B paths only (see the conduction paths, for example of collinear phases A and C in Figs. 4 and 5 respectively). In this case all the phases have an atomic level located at $\epsilon_{B'}(= 0)$ in the limit $J \to \infty$. This is directly seen in the density of states (DOS) of these phase. In Fig. 10 we show the DOS for the F, A, C, "flux" and paramagnet phases. This dispersion-less level gives constant T_c in density region $n = [1, 2]$. This feature, and several others, are modified by finite B′B′ hopping, which leads to broadening of this level. It makes the DOS of the various magnetic phases asymmetric (in energy) and also destroys the particle-hole symmetry in the phase diagram.

3.2. *Variational scheme*

Using the approach discussed earlier, we found the ground state configurations at different electron densities. In this set we also get certain spiral phases, which are small variations of FM, A and C phases in the left and right part of the density window. Since in these parts MC also gives (for FM, A) clean result, we interpret it as a finite size effect. To get convinced about it, we compare the energies of these collinear phases (FM, A, C) with all their neighboring modulations $\delta\mathbf{q}$s, at various lattice sizes. We find that with increasing lattice size, the per particle energy difference between collinear phase, and lowest energy candidate with the neighboring $\mathbf{q}_\theta$, $\mathbf{q}_\phi$, decreases, which convinces us that if we go to large enough lattice size, this difference will eventually vanish and the collinear phases (F, A, C) will be the relevant candidates.

We use a similar scheme for the middle part, however there no simple phase suggested by this variational scheme (neither by MC). The phases we propose for

[b]We campared ratio of the maximum of $(\delta E)^{\rm FM}$ and maximum of $(\delta E)^{\rm AF}$ in the density window, for $\Delta = 0$ and $t' = 0$.

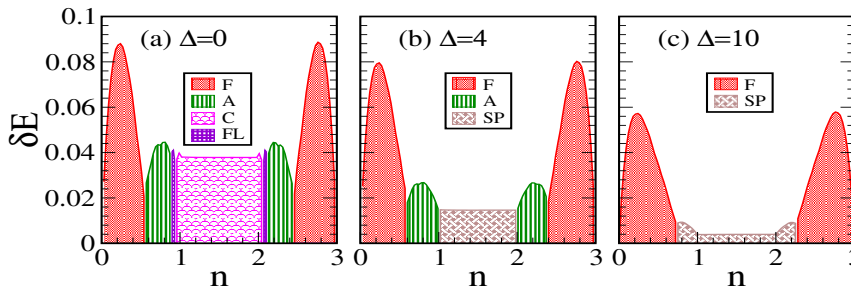

Fig. 9. (Color online) The energy difference δE of ground-state and paramagnetic phase. A variational estimate of the T_c for three values of (a) $\Delta = 0$, (b) $\Delta = 4$, (c) $\Delta = 10$ and $t' = 0$. The sequence of phases from low density to middle is FM, A, C and "flux" ($\Delta = 0$) or spiral ($\Delta = 4, 10$). The decrease in the "T_c" with Δ is more drastic in AF phases.

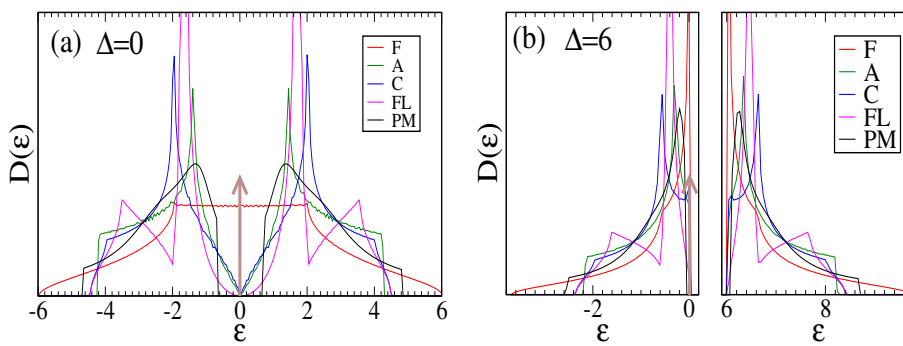

Fig. 10. (Color online) DOS for the F, A, C, FL ("flux") and PM (paramagnetic) phases. (a) for $\Delta = 0$ and (b) for $\Delta = 6$. In order of decreasing band width are phase F, PM, C, FL and A (FL and C have same bandwidth). This is for both $\Delta = 0, 6$, and the order in general does not depend on the Δ. The plot for $\Delta = 6$ is split in two parts, with the region between $\epsilon = [0, 6]$, with zero weight, omitted. The δ function arises from the localized B$'$ level.

the middle density part based on this variational scheme are SP_1, SP_2, SP_3 and "flux". See the configurations in Fig. 6 and $S(\mathbf{q})$ details from Table 1.

In Fig. 2, the magnetic ground state is shown for $t' = 0$ and $t' = 0.3$ (top and bottom). We see that for $t' = 0$ the phase diagram is symmetric in density. For small Δ, in the range $0 - 4$, we have FM, followed by A-type, C-type and "flux" phase. The order reverses as we go in the other half of the density window. The G-type phase which was largest stable phase in 2D (Figs. 2 and Fig. 5 in Ref. 19) is almost taken over by the "flux" phase. The stability of the "flux" phase decreases with Δ and it does not show up for $\Delta > 4$.

In Fig. 10, we show the DOS for F, A, C "flux" and PM phases. The upper and the lower panel correspond to $\Delta = 0$ and $\Delta = 6$ respectively. In all the phases, at all Δ, there is a spike (delta function) at $\epsilon = 0$, which accounts for the nondispersive level at $\epsilon_{B'} = 0$.

For FM all the core spins are ↑ (say), so only ↓ spin electrons from B′ site get to delocalize while ↑ spin electrons remain localized at $\epsilon = 0$, which corresponds to the localized band in the spectrum and the spike in the DOS. So the localized level in FM is an ↑ spin level. The nature of this localized level however changes when we go to AF phases. In collinear phases, its easy to understand the nature of this localized band. Take for example the case of A-type in Fig. 4 down panel with conduction path. The lattice is divided into two sub-lattices (each of which are of layered zigzag shape), blue and red, such that, if (say) core spins in the f sites in the blue sub-lattice are all ↑, then the same in red sub-lattice are ↓. As a result, in the blue sub-lattice, ↓ spin electrons get to delocalize, while ↑ spin electron remain localized. The opposite happens in the red sub-lattice. Since these lattices are disconnected from each other, one can separately diagonalize them. But each of this sub-lattice, however complicated in shape, is a FM, so it gives 1/3 of the levels localized at $\epsilon = 0$, which will be ↑ spin in blue sub-lattice, while it will be ↓ spin in red sub-lattice. Since both the sub-lattices have same number of sites/unit cells, we get 1/3 of the levels localized at $\epsilon = 0$ but now spin degenerate. The delocalized states have also to be spin-degenerate, and their nature depends on the way the conduction paths divide the lattice into two sub-lattices.

For each spin channel the conduction paths are layered zigzag, 2D in the A-type phase, while they are 3D in the C-type phase.

This appearance of the localized band is not restricted to just the collinear phases, but also happens for noncollinear phases, and even the paramagnet.

4. Results: Particle-Hole Asymmetry

The model with only "nearest neighbor" (BB′) hopping has a rich phase diagram. However, this has the artificial feature of a nondispersive level. In reality all materials have some degree of B′B′ hopping and we wish to illustrate the qualitative difference that results from this hopping. We explored two cases, $t' = 0.3$ and $t' = -0.3$ for these particle-hole asymmetric cases.

4.1. *Monte Carlo*

In Figs. 11(a) and 11(b) we show the structure factor data, at two densities, for (a) A-type and (b) C-type phases, to demonstrate one remarkable difference from the particle-hole symmetric case. As we saw earlier in Fig. 7 for $t' = 0$ the structure factor data were very noisy for AF phases, with many sub-dominant $\mathbf{q}$ peaks around the central peak. The saturation value for the A-type peak in the symmetric case was $\sim 10^{-2}$, while now it is ~ 0.2, close to the ideal value of 0.25. The sharp change in the structure factor makes the identification of the T_c scale more reliable. Although inclusion of t' does not remove the noise completely, it is reduced over a reasonable part of the phase diagram.

Figure 12(a) presents the $n-T_c$ phase diagram for $t' = 0.3$ and $\Delta = 0$ established from MC, along with the δE from the variational approach [Fig. 12(b)]. In this

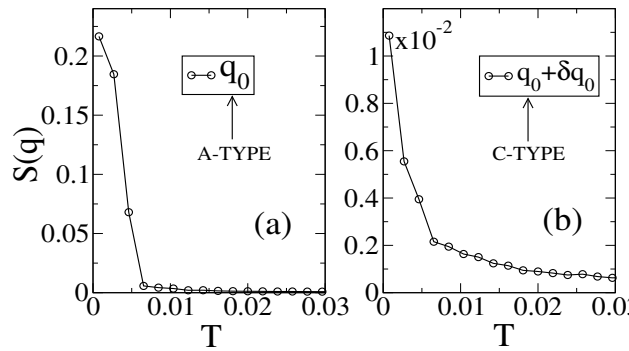

Fig. 11. $S(\mathbf{q})$ for $t' = 0.3$ and $\Delta = 0$ at (a): a typical density $n \sim 0.5$ for A-type phase and (b): a typical density $n \sim 1.2$ for C-type phase. A demonstration of $S(\mathbf{q})$ with no sub-dominant peaks, unlike at $t' = 0$.

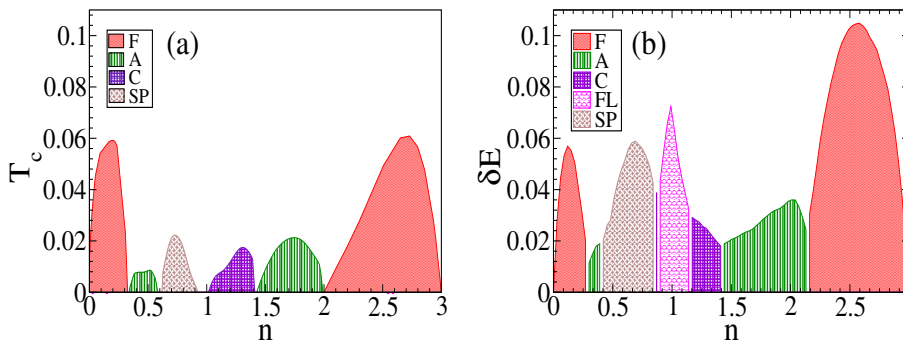

Fig. 12. (Color online) Phase diagram obtained via MC (left) and from the variational calculation (right) at $t' = 0.3$ and $\Delta = 0$.

case, the phases that appear as a function of density n are FM, A-type, spiral, C-type, A-type and FM again. For FM, the window of stability gets reduced in the left (low density) part but enhanced to almost full band ($n \sim 2$ to 3) in the right (high density) part. The $\uparrow\uparrow\downarrow\downarrow$ phase appears again, but being a finite size artifact, is absorbed in the FM (and not shown). The T_c is usually reduced, from the symmetric ($t' = 0$) case, as BB′ hopping provides conduction paths that are nonmagnetic. There is a wider space with moderate T_c for A-type phase, located asymmetrically in density. It is more stable, in the right window, than left window, hence possessing relatively higher T_c than left. The correlations of spiral and C-type phases are also captured with relatively less noise, see Fig. 11(b) for example of C-type correlation. Although $S(\mathbf{q})$ data for these phases still contain some noise, so that we don't get clean ground state here either. The $n - T$ phase diagram for $t' = -0.3$ and $\Delta = 0$, can be obtained from transformation $n \to 3 - n$, i.e., reversing the density axis of Figs. 12(a) and 12(b).

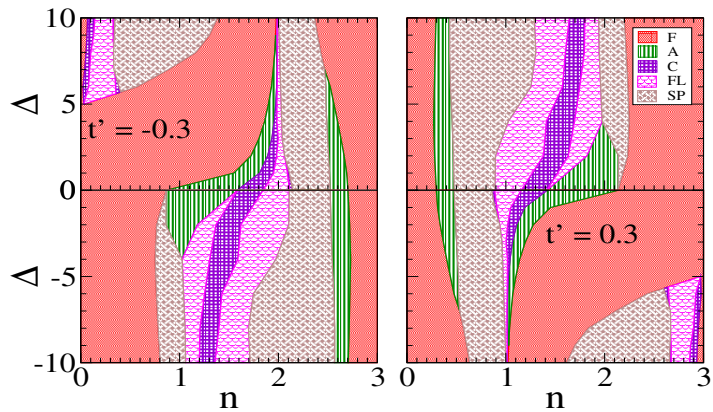

Fig. 13. (Color online) Ground state phase diagram in the presence of $t' = \pm 0.3$.

4.2. *Variational scheme*

We employ the variational scheme discussed earlier and obtain the ground state phase diagram for $t' = \pm 0.3$ is shown in Fig. 13. Turning on t' has a significant effect on the phase diagram, when we use the $t' = 0$ case, Fig. 2 top panel, for reference. The particle hole symmetry ($n \to 3 - n$) is destroyed at finite Δ but a reduced symmetry $(n, \Delta, t') \to (3 - n, -\Delta, -t')$ still holds. The phase diagram is richer in the middle of the density window where crossing among various phases occurs at different densities. Due to the symmetry mentioned above it is enough to discuss the $\Delta > 0$ case with $t' = \pm 0.3$.

For $t' = 0.3$ the trends from MC are well reproduced by the variational scheme on large (20^3) systems at $\Delta = 0$. We observe reduced stability of FM at low density and enhancement at high density.

Note that the overall correspondence between the Monte Carlo and the variational approach is much better here than in the $t' = 0$ case, Fig. 8 and Fig. 9.

The A-type phase becomes very thin in the left, but unaffected by Δ, while in right side it widens up in the low Δ and gets replaced by the spiral quickly as we go up in Δ. "flux" and C-type both become stable for high Δ with a gradual shift in the high density. For $t' = -0.3$, at very small Δ in the left and the middle part A-type and the spiral are major candidates with small window for C–AF and "flux". The behavior in this part is not very sensitive to sign of t'.

Focusing on $t' = -0.3$, as go up from $\Delta = 0$ to $\Delta \sim 5$ the AF phases become less and less stable and are almost wiped out from the left part of the density, and FM becomes stable there. The largest stability window of FM occurs roughly near $\Delta \sim 5$, where its stable up-to $n \sim 1.8$. Going further with higher Δ, FM looses its stability, from C-type, "flux" and spirals. However, there is very thin strip of stability of the FM in the band edge in the left part, and towards the middle density, there is re-entrance of the FM phase.

In the right part of the density, we have FM, A-type and spiral. Increasing Δ

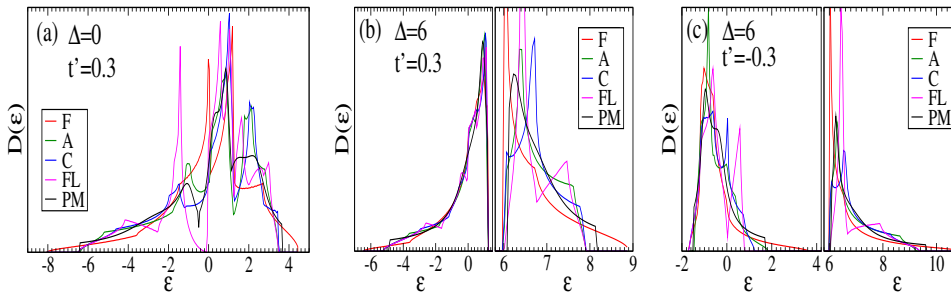

Fig. 14. (Color online) DOS for the F, A, C, FL, PM phases (a) $\Delta = 0$, $t' = 0.3$, there is no resemblance to the particle-hole symmetric case. FM and PM have largest bandwidth, while A, C, "flux" have almost same bandwidth (b) $\Delta = 6$, $t' = 0.3$, due to large band-gap, two bands are shown in two different panels (left, right) the same bandwidth order, right band less effected from t', being situated around Δ (c) $\Delta = 6$, $t' = -0.3$. The structure of the band edges has changed drastically. Now band edges of the FM, "flux" and C-type coincide on the left, while on the right edge of the first panel FM is more widespread.

reduces the stability of A-type to FM, making it vanish near $\Delta \sim 7$, while FM window keeps increasing with Δ.

The DOS for the ordered F, A, C, "flux" phase and the paramagnet are shown in Fig. 14. (a) For $t' = 0.3$, $\Delta = 0$ FM has the largest bandwidth, with paramagnet second largest. The band edges of A, C, "flux" almost coincide both for small and large Δ. (b) For $t' = 0.3$, $\Delta = 6$ the left band shows that all the phases seem to have 'almost' similar features in the DOS, while the right band shows distinct features of each of the phases, similar to $t' = 0$ DOS. (c) For $t' = -0.3, \Delta = 6$ however, has a distinct case. Here the lower edge of the band for FM, "flux" and C coincide, and the DOS of "flux", or C, is higher than FM, which explains why FM becomes unstable in the left side and taken by "flux" and C, upon increasing Δ.

We also estimate the PS boundaries between FM, A, C phases shown in Fig. 15. For $t' = 0$ and for $\Delta > 0$, we see that PS regions are significant, while they vanish for $\Delta < 0$ as we go down. For $t' = 0.3$, (right panel) the PS boundaries are too narrow to be visible.

In Fig. 16 we have shown the $\delta E(n)$ calculated for 20^3 size, for $\Delta = 4$, $t' = -0.3$, with the large stability window of ferromagnet (see Fig. 12). Here, though the Δ and t' are nonzero, due to unusually large stability window, the δE (or T_c) is large.

To summarize, from the MC and variational data we learn that, apart from asymmetry in the phase diagram, collinear FM and A-type phases become stable in wide density window. Their T_c however is slightly reduced than the symmetric case. The $S(\mathbf{q})$ data showing less noise for A-, C-type and spirals indicates that the energy landscape become "smoother" by t' so that annealing process becomes easier to get to the ground state. The energy differences δE as well as MC estimated T_cs show overall decrease with t'. This is understandable as, by introducing t' we allow electrons to more on the "nonmagnetic" sub-lattice B′. Now the energy of any phase, depends on the energy gain via the hopping process. From the nearest

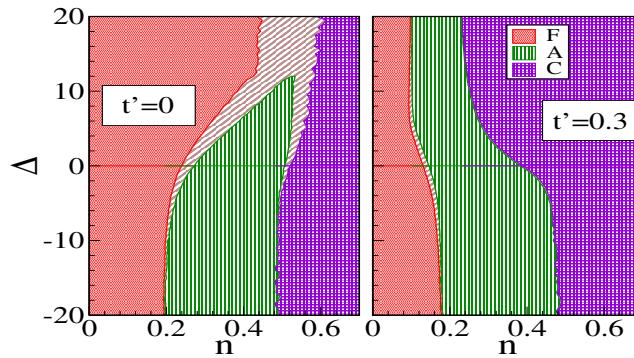

Fig. 15. (Color online) PS regions. left column for $t' = 0$ and right column of $t' = 0.3$. Notice that PS regions are significant for $\Delta > 0$ and $t' = 0$, for $t' \neq 0$ and for $\Delta < 0$ PS boundaries almost vanish.

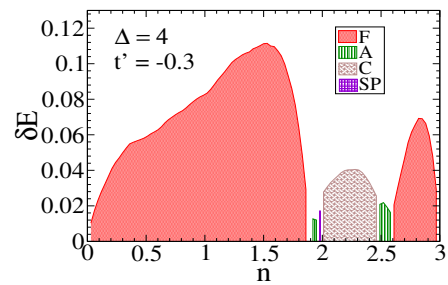

Fig. 16. (Color online) Asymmetric case, the energy difference δE of ground-state and paramagnetic phase. Top: $\Delta = 4$, $t' = -0.3$ where FM is stable in the large portion of the density. Bottom: $\Delta = 0$, $t' = 0.3$ The trends of δE match with T_c.

$f - m$ hopping, this gain scales as t^2/Δ subject to spin configurations, while from the next nearest $m - m$ hopping, this gain simply scales as t', and does not care upon spin configurations. So more we increase t' and Δ, the more we are making the energy of the system insensitive to spin-configurations. The asymptotic limit of this is $(t^2/\Delta) \to 0$ when every phase has same energy as paramagnet. That also explains why the PS windows become very small with inclusion of t'.

In the couple of paragraphs below we try to create an understanding of how the phase diagram is affected by t'. There is not, unfortunately, an understanding of the effects over the entire density window, but we can at least motivate the changes at low density.

For $t' = -0.3$, the FM loses its stability to AF phases even at low n. That is puzzling since one would expect the FM phase to have the largest bandwidth. We recall that in the $t' = 0$ case, there is a localized band coming from B$'$ level for all the phases. The dispersion of this previously localized level causes the m and f to have a $\mathbf{k}$ dependent separation, which was Δ for all $\mathbf{k}$ in the symmetric case. The separation for these levels in the asymmetric case is $\Delta_{\mathbf{k}} = \Delta - \epsilon'_{\mathbf{k}}$, which

varies from $\Delta - 12|t'|$, to $\Delta + 12|t'|$ in 3D. In 2D it varies from from $\Delta - 4|t'|$, to $\Delta + 4|t'|$.

If we consider the simpler 2D case for illustration, $\epsilon'_{\mathbf{k}} = -4t' \cos k_1 \cos k_2$, which, for $t' > 0$ is minimum at $\mathbf{k} = (0,0), (\pi,\pi)$ while the maximum is at $\mathbf{k} = (\pi,0), (0,\pi)$. For $t' < 0$ the opposite will happen. Thus, for $t' > 0$ $\mathbf{k} = (0,0), (\pi,\pi)$ and neighboring states will experience enhanced mixing $\sim \Delta - 4|t'|$, while, the states near $\mathbf{k} = (\pi,0), (0,\pi)$ experience lower mixing. In the ferromagnet (both in 2D and 3D), the lowest eigenvalue corresponds to $\mathbf{k} = (0,0)$, while (for 2D) the G-type phase has lowest eigenvalues at $\mathbf{k} = (0,0), (\pi,0)(0,\pi)(\pi,\pi)$. Therefore, for $t' < 0$, the lowest eigenvalues of both the phases are enhanced but the band-edge of FM stays lower than G-type. While in the other, the strongest mixing states are $(\pi,0)$ and $(0,\pi)$, which are not at the edge for FM, its band-edge gets lower enhancement, while the band-edge of G type gets lowered. For a given t', as we increase Δ, a point comes where band edges of the FM and G, coincide. This is the point where FM loses its stability.

The same argument can be extended to 3D, with C and flux phases, just the role of the qs gets extended to 3D (e.g., $(\pi,0,0)$ etc), and the correction in the separation is $\sim 12t'$ instead of $\sim 4t'$. In Fig. 17 we have shown the plot of lowest eigenvalues of F, A, C and flux phases with Δ for $t' = \pm 0.3$.

Finally, a comment (mainly a conjecture), Fig. 18, on how the energy landscape of the DP model changes on addition of t'. We already know that the "binding energy" and T_c of magnetic phases reduce with increasing t' — but also that the "noise" in the cooling process also reduces quickly.

If $t' \gg t$ then the electrons could delocalize on the wide t' based band populating the nonmagnetic sites only. Magnetic order would make little difference to electronic energies and the "energy landscape" in the space of spin configurations would be featureless, Panel (c) in Fig. 18. There are no global minima, i.e., ordered states, and no local minima either. If $t' = 0$ then delocalization takes place necessarily through the magnetic sites and the deep minima in configuration space represent ordered states while the "grassy" features indicate shallow metastable states close

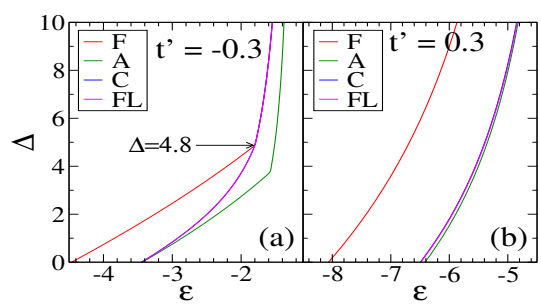

Fig. 17. (Color online) Asymmetric case, lowest eigenvalues plotted as function of Δ for the F,A,C and flux phases calculated from the dispersions. (a) $t' = -0.3$ and (b) $t' = 0.3$.

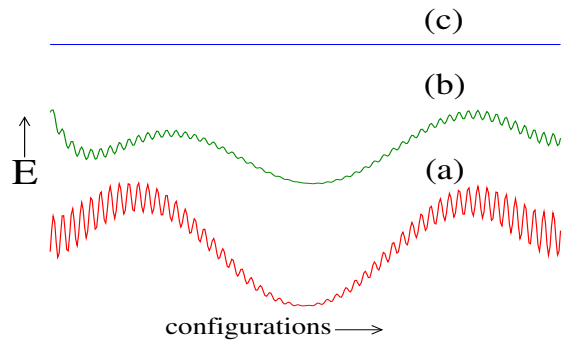

Fig. 18. (Color online) A schematic energy landscape of the DP model, in the space of spin configurations, for (a) $t'/t = 0$ (bottom), (b) $t'/t \sim \mathcal{O}(1)$ (middle) and (c) $t'/t \to \infty$ (top). The panels are indicated for a fixed set of electronic parameters, except t' which varies as indicated above. At $t' = 0$ the landscape has many local minima around the deep minimum, and while the "binding energy" of the ordered state, with respect to the paramagnet, is large (and so also the T_c) the system is apt to get stuck in one of the neighboring minima in the cooling process. When $t'/t \to \infty$ magnetic order makes no difference to the energy, the electrons bypass the magnetic sites. At intermediate t', while the binding energy and T_c are smaller, the local minima also seem to be fewer and shallower. This makes the ordered state easier to access.

to them. Our MC data probing AF states at $t' = 0$ suggests this picture, curve (a) in Fig. 18. At intermediate t' the ordered states are shallower, but the metastable states seem to have been affected even more drastically, if our MC data, Fig. 11, is to be taken seriously.

While the discussion above seems to be merely an analysis of trends in the MC annealing process, a simpler energy landscape would make the occurrence of AF states more likely in the real materials as well.

5. Discussion

The real DPs are multi-band materials, involving additional interaction effects and antisite disorder beyond what we have considered in this paper. Nevertheless, we feel it is necessary to understand in detail the phase diagram of the "simple" model we have studied, and then move to more realistic situations. In what follows, we first provide a qualitative comparison of the trends we observe with experimental data, and then move to a discussion of issues that are ignored in the present model.

The t_{2g} orbitals in the DPs are three-fold degenerate and this is a major difference with respect to the model we have studied. At the simplest level it requires a renormalization of the electron count to relate our results to real materials. We do this first, below. Orbital effects can also *qualitatively* change the phase diagram, as in the manganites, we comment on that later.

Comparison to experiments: There is limited experimental signature[23] of metallic AF phases driven by the kind of mechanism that we have discussed. So, the comparison to experiments is, at the moment, confined to the T_c scales[24,25] etc, of the ferromagnetic DP's. In a material like SFMO the electron density can be

increased by doping La for Sr, i.e., compositions like $Sr_{2-x}La_xFeMoO_6$. This was tried[24] and the T_c increased from 420 K at $x = 0$ to $\sim$ 490 K at $x = 1$. SFMO has threefold degeneracy of the active, t_{2g}, orbitals while we have considered a one band model. When we create a correspondence by dividing the electron count by the maximum possible per unit cell (3 in our case, 9 in the real material), in our units $x = 0$ corresponds to $n = 0.33$ and $x = 1$ to $n = 0.66$.

When $t' = 0$, as a function of n the T_c peaks around $n = 0.2$, Fig. 8, quite far from the experimental value. However, in the presence of $t' = -0.3$ and $\Delta = 4$, Fig. 16, the peak occurs above $n = 1$. So, modest t' can generate the ferromagnetic window that is observed, and produce a $T_c \sim 0.1t$. For $t = 0.5$ eV, this is in the right ballpark.

Effect of orbital variables: Apart from renormalization of the electron count, multiple orbitals could, in principle, have a qualitative effect. If the local orbital degeneracy is lifted by Jahn–Teller or Coulomb effects then the resulting "orbital moment" could order in some situations. This orbital ordered (OO) background can modify electron propagation and the magnetic state. This is known to happen at some dopings in the manganites. Even there, however, the broad sequence of magnetic phases is consistent with predictions from a one band model. The DPs do not seem to involve strong lattice effects, the orbital degeneracy survives, and there is no orbital order. This suggests that there is even better chance of a one-band model being qualitatively correct here, compared to the manganites.

Had there been strong OO effects, the spin–spin coupling in that background may have picked up strong directionality, and the geometric frustration may not have been relevant. This does not seem to be relevant in most DPs. Indeed, there are experiments on the insulating DP's[27–29] where the geometric frustration of the FCC lattice leads to a nontrivial magnetic state, unrelieved by the presence of multiple orbitals.

We of course expect that the phase boundaries and T_c scales that we calculate would be affected by the orbital degeneracy. However, the trends in the phase diagram with increasing density simply reflect a growing AF tendency and the non coplanar phases emerge due to the impossibility of G-type order. This trend should be independent of number of orbitals, although the specific noncoplanar phase may not be "flux" like.

Antisite disorder: Attempts to increase n via A site substitution also brings in greater antisite disorder (B–B′ interchange) and even the possibility of newer patterns of A site ordering (!) complicating the analysis. For example, one would try compositions of the form: $A_{2-x}A'_xBB'O_6$, where A and A′ have different valence in an attempt to change n. The assumption is that the A′ only changes n without affecting other electronic parameters, i.e., A′ ions do not order and remain in an alloy pattern. This may not be true. In fact, at $x = 1$, the material $AA'BB'O_6$ may have a specific A–A′-B–B′ ordering pattern that affects electronic parameters in a nontrivial way and one cannot understand this material as a perturbation on $A_2BB'O_6$. In such a situation one needs guidance from experiments and *ab initio*

theory to fix electronic parameters as x is varied. All this before one even considers the inevitable antisite (B–B′) disorder and its impact on magnetism.[26]

6. Conclusions

We have studied a one band model of DPs in three dimensions in the limit of strong electron-spin coupling on the magnetic site. The magnetic lattice in the cubic DPs is FCC and increasing the electron density leads from the ferromagnet, through A- and C-type collinear antiferromagnets, to spiral or "flux" phases close to half-filling. We estimate the T_c of these phases, via MC and variational calculation, and find the AF T_c to be significantly suppressed compared to the 2D case. We attribute it to the geometric frustration on the FCC lattice. The introduction of B′B′ hopping $t'/t \sim 0.3$ significantly alters the phase diagram and T_c scales and creates a closer correspondence to the experimental situation on DP ferromagnets.

Acknowledgments

We acknowledge use of the high performance computing facility at HRI. PM was supported by a DAE-SRC Outstanding Research Investigator Award, and the DST India via the Indo-EU ATHENA project. RT acknowledges the use of Asymptote[30] to generate 3D graphics used as figures.

Appendix A. Dispersion for Ordered Phases

Here we show how to calculate dispersion for selected ordered phases, which have relatively small unit cells. We define the unit cell for each phase, and go to k-space where the Hamiltonian becomes block diagonal.

A.1. *Spectrum for collinear phases*

The Hamiltonian can be diagonalized by Fourier transformation. We write the Hamiltonian H as $H = H_0 + H_J$, where, H_0 is given by:

$$H_0 = \sum_{\mathbf{X}\sigma}[\epsilon_1 f^\dagger_{\mathbf{X},\sigma} f_{\mathbf{X},\sigma} + \epsilon_2 m^\dagger_{\mathbf{X}+\mathbf{a_1},\sigma} m^\dagger_{\mathbf{X}+\mathbf{a_1},\sigma}] - t \sum_{\mathbf{X},\sigma,\boldsymbol{\delta}\in \mathrm{NN}} (f^\dagger_{\mathbf{X},\sigma} m_{\mathbf{X}+\boldsymbol{\delta},\sigma} + \mathrm{h.c.})$$
$$- t' \sum_{\mathbf{X},\sigma,\boldsymbol{\delta}\in \mathrm{NNN}} (m^\dagger_{\mathbf{X}+\mathbf{a}_1,\sigma} m_{\mathbf{X}+\mathbf{a}_1+\boldsymbol{\delta},\sigma} + \mathrm{h.c.}) \tag{A.1}$$

and H_J is given by:

$$H_J = J \sum_{\mathbf{X}} \mathbf{S}(\mathbf{X}) \cdot \boldsymbol{\sigma}_{\alpha,\beta} f^\dagger_{\mathbf{X},\alpha} f_{\mathbf{X},\beta}\,. \tag{A.2}$$

The lattice vector $\mathbf{X}$ is defined as $\mathbf{X} = n_1\mathbf{A}_1 + n_2\mathbf{A}_2 + n_3\mathbf{A}_3$ with $A_i, i = 1, 2, 3$ as the primitive lattice vectors ($A_1 = (2, 0, 0)$, $A_2 = (1, 1, 0)$, $A_3 = (0, 1, 1)$), defining the periodicity of lattice with the 2 site unit cell. With this periodicity, the unit

cell has one "f" and one "m" site at $(0,0,0)$ and $(1,0,0)$ respectively. Now doing a Fourier transform on "f" operators (similarly for "m"s)

$$f^{\dagger}_{\mathbf{X},\sigma} = \frac{1}{\sqrt{N}} \sum_{\mathbf{k}} f^{\dagger}_{\mathbf{k},\sigma} \exp(i\mathbf{k}\cdot\mathbf{X})\,. \tag{A.3}$$

This simplifies the nonmagnetic part H_0 as follows:

$$\begin{aligned} H_0 &= \sum_{\mathbf{k},\sigma} [(\epsilon_2 + A'_{\mathbf{k}}) m^{\dagger}_{\mathbf{k},\sigma} m_{\mathbf{k},\sigma} + \epsilon_1 f^{\dagger}_{\mathbf{k},\sigma} f_{\mathbf{k},\sigma} + (A_{\mathbf{k}} f^{\dagger}_{\mathbf{k},\sigma} m_{\mathbf{k},\sigma} + \text{h.c.})] \\ &= \sum_{\mathbf{k},\sigma} (f^{\dagger}_{\mathbf{k},\sigma} m^{\dagger}_{\mathbf{k},\sigma}) \begin{pmatrix} \epsilon_1 & A_{\mathbf{k}} \\ A_{\mathbf{k}} & \epsilon_2 + A'_{\mathbf{k}} \end{pmatrix} \begin{pmatrix} f_{\mathbf{k},\sigma} \\ m_{\mathbf{k},\sigma} \end{pmatrix}, \end{aligned} \tag{A.4}$$

which is reduced to 2×2 block. The amplitudes $A_{\mathbf{k}} = -2t(\cos k_x + \cos k_y + \cos k_z)$ and $A'_{\mathbf{k}} = -4t'(\cos k_x \cos k_y + \cos k_y \cos k_z + \cos k_z \cos k_x)$ are just the cubic and FCC dispersions.

Next, we have to simplify the H_J part. For the collinear phases, $\mathbf{S}(\mathbf{X})$ can be expressed as $\mathbf{S}(\mathbf{X}) = (0,0,e^{i\mathbf{q}\cdot\mathbf{X}})$. For FM, $\mathbf{q}$ is trivially $(0,0,0)$. For A-type, $\mathbf{q} = (\pi/2, -\pi/2, \pi/2)$, while for C-type $\mathbf{q} = (0,\pi,-\pi)$. Now, plugging this value of $\mathbf{S}(\mathbf{X})$ in H_J and doing the Fourier transform for the H_J, we get,

$$H_J = J \sum_{\mathbf{k}} \sigma f^{\dagger}_{\mathbf{k},\sigma} f_{\mathbf{k}+\mathbf{q},\sigma}\,; \quad \sigma = \pm 1\,. \tag{A.5}$$

Now $\mathbf{q} = 0$ for FM, so H_J becomes diagonal. Thus total Hamiltonian H still remains 2×2 block, and the eigenvalues for the FM are solutions of the following 2×2 block,

$$H_{2\times 2}(\mathbf{k},\sigma) = \begin{pmatrix} \epsilon_1 + J\sigma & A_{\mathbf{k}} \\ A_{\mathbf{k}} & \epsilon_2 + A'_{\mathbf{k}} \end{pmatrix}. \tag{A.6}$$

For A-type and C-type phases, we get matrix elements connecting $|\mathbf{k},\sigma\rangle \to |\mathbf{k}+\mathbf{q},\sigma\rangle \to |\mathbf{k},\sigma\rangle$, so that now we get to solve following 4×4 block

$$H_{4\times 4}(\mathbf{k},\sigma) = \begin{pmatrix} \epsilon_1 & J\sigma & A_{\mathbf{k}} & 0 \\ J\sigma & \epsilon_1 & 0 & A_{\mathbf{k}+\mathbf{q}} \\ A_{\mathbf{k}} & 0 & \epsilon_2 + A'_{\mathbf{k}} & 0 \\ 0 & A_{\mathbf{k}+\mathbf{q}} & 0 & \epsilon_2 + A'_{\mathbf{k}} \end{pmatrix} \tag{A.7}$$

From these we obtain the spectrum for F, A, C phases on large ($\sim 100^3 - 500^3$) lattices, which can be used to calculate the DOS, phase diagram, PS windows etc.

A.2. *Spectrum for the "flux" phase*

The unit cell for the "flux" phase has 4B, and 4B′ atoms lying on the corners of the cube. The primitive lattice vectors become $A_i = \{(2,0,0),(0,2,0),(0,0,2)\}$ At finite J, the same procedure (as for collinear phases) will reduce the Hamiltonian

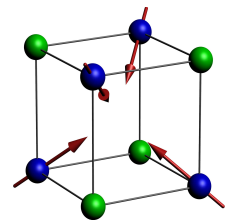

Fig. A.1. Unit cell structure for the Flux phase.

into 16×16 block. To make life a bit simple, we use the $J \to \infty$ limit on the Hamiltonian for the "flux" phase, which is same as used in Ref. 19 except its the 3D version.

This gives us four spin-less f_i levels and 8 $m_{i,\sigma}$ levels in the unit cell, which upon simplification reduces to 12×12 block. With the basis $(f_i(k)m_{i\uparrow}(k))_{i\in\{1,2,3,4\}}$. The Hamiltonian breaks into 12×12 block given as follows:

$$H = \begin{pmatrix}
\Delta & 0 & 0 & 0 & t_{1\uparrow}a_1 & t_{1\downarrow}a_1 & t_{1\uparrow}a_2 & t_{1\downarrow}a_2 & 0 & 0 & t_{1\uparrow}a_3 & t_{1\downarrow}a_3 \\
0 & \Delta & 0 & 0 & t_{2\uparrow}a_2 & t_{2\downarrow}a_2 & t_{2\uparrow}a_1 & t_{2\downarrow}a_1 & t_{2\uparrow}a_3 & t_{2\downarrow}a_3 & 0 & 0 \\
0 & 0 & \Delta & 0 & t_{3\uparrow}a_3 & t_{3\downarrow}a_3 & 0 & 0 & t_{3\uparrow}a_2 & t_{3\downarrow}a_2 & t_{3\uparrow}a_1 & t_{3\downarrow}a_1 \\
0 & 0 & 0 & \Delta & 0 & 0 & t_{4\uparrow}a_3 & t_{4\downarrow}a_3 & t_{4\uparrow}a_1 & t_{4\downarrow}a_1 & t_{4\uparrow}a_2 & t_{4\downarrow}a_2 \\
t^*_{1\uparrow}a_1 & t^*_{2\uparrow}a_2 & t^*_{3\uparrow}a_3 & 0 & 0 & 0 & t_{12} & 0 & t_{23} & 0 & t_{13} & 0 \\
t^*_{1\downarrow}a_1 & t^*_{2\downarrow}a_2 & t^*_{3\downarrow}a_3 & 0 & 0 & 0 & 0 & t_{12} & 0 & t_{23} & 0 & t_{13} \\
t^*_{1\uparrow}a_2 & t^*_{2\uparrow}a_1 & 0 & t^*_{4\uparrow}a_3 & t_{12} & 0 & 0 & 0 & t_{13} & 0 & t_{23} & 0 \\
t^*_{1\downarrow}a_2 & t^*_{2\downarrow}a_1 & 0 & t^*_{4\downarrow}a_3 & 0 & t_{12} & 0 & 0 & 0 & t_{13} & 0 & t_{23} \\
0 & t^*_{2\uparrow}a_3 & t^*_{3\uparrow}a_2 & t^*_{4\uparrow}a_1 & t_{23} & 0 & t_{13} & 0 & 0 & 0 & t_{12} & 0 \\
0 & t^*_{2\downarrow}a_3 & t^*_{3\downarrow}a_2 & t^*_{4\downarrow}a_1 & 0 & t_{23} & 0 & t_{13} & 0 & 0 & 0 & t_{12} \\
t^*_{1\uparrow}a_3 & 0 & t^*_{3\uparrow}a_1 & t^*_{4\uparrow}a_2 & t_{13} & 0 & t_{23} & 0 & t_{12} & 0 & 0 & 0 \\
t^*_{1\downarrow}a_3 & 0 & t^*_{3\downarrow}a_1 & t^*_{4\downarrow}a_2 & 0 & t_{13} & 0 & t_{23} & 0 & t_{12} & 0 & 0
\end{pmatrix},$$

where the symbols in the above are defined as:

$$\alpha = \sqrt{\frac{\sqrt{3}+1}{2\sqrt{3}}}\,; \quad \beta = \sqrt{\frac{\sqrt{3}-1}{2\sqrt{3}}}\,; \quad z = \frac{1-i}{\sqrt{2}}\,;$$

$$a_1 = 2\cos k_1\,; \quad a_2 = 2\cos k_2\,; \quad a_3 = 2\cos k_3\,;$$

$$t_{12} = -4t'\cos k_1 \cos k_2\,; \quad t_{23} = -4t'\cos k_2 \cos k_3\,; \quad t_{13} = -4t'\cos k_1 \cos k_3\,;$$

$$t_{1\uparrow} = t_{2\uparrow} = -t\alpha\,; \quad t_{3\uparrow} = t_{4\uparrow} = -t\beta\,; \quad t_{1\downarrow} = -t_{2\downarrow} = tz\beta\,;$$

$$t_{3\downarrow} = -t_{4\downarrow} = -tz^*\alpha\,.$$

This gives us $H(\mathbf{k})_{12\times12}$, which is very difficult to diagonalize analytically, but still saves us from diagonalizing full real-space matrix of $\mathcal{O}(\mathcal{N})$ size, and reduces the problem to $\mathcal{O}(\mathcal{N})$ number of diagonalizations of 12 sized matrix.

The comparison of energies using the $\epsilon_{\mathbf{k}}$ obtained for F, A, C and flux phases, one can draw the magnetic phase diagram for large lattice size ($N \sim 400^3$). The

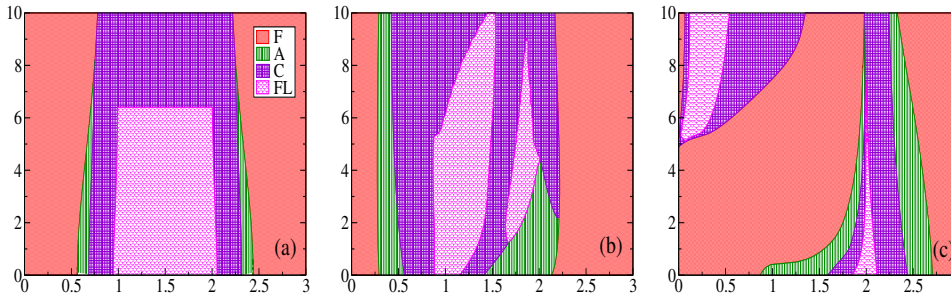

Fig. A.2. (Color online) Phase diagram based on k space based diagonalization for $t' = 0, 0.3, -0.3$. System size $N = 160^3$. Here we can only use F, A, C and "flux" phase as candidate states but some of the complexity of more elaborate phase diagrams, Fig. 2, are already present.

Fig. A.2, shows the phase diagram, which can be compared to that obtained through real space calculations done on 20^3 size.

References

1. D. D. Sarma, *Current Op. Solid St. Mat. Sci.* **5**, 261 (2001).
2. D. Serrate, J. M. de Teresa and M. R. Ibarra, *J. Phys. Cond. Matt.* **19**, 023201 (2007).
3. M. T. Anderson *et al.*, *Prog. Solid State Chem.* **22**, 197 (1993).
4. K.-I. Kobayashi *et al.*, *Nature* **395**, 677 (1998).
5. M. A. Subramanian, N. S. Rogado and J. Li, *Adv. Mater.* **17**, 2225 (2005).
6. H. Das *et al.*, *Phys. Rev. Lett.* **100**, 186402 (2008).
7. H. Das, M. De Raychaudhury and T. Saha-Dasgupta, *Appl. Phys. Lett.* **92**, 201912 (2008).
8. D. D. Sarma *et al.*, *Phys. Rev. Lett.* **85**, 2549 (2000).
9. J. B. Philipp *et al.*, *Phys. Rev. B* **68**, 144431 (2003).
10. P. Majewski *et al.*, *Phys. Rev. B* **72**, 132402 (2005).
11. Y. Krockenberger *et al.*, *Phys. Rev. B* **75**, 020404 (2007).
12. T. K. Mandal *et al.*, *Phys. Rev. B* **78**, 134431 (2008).
13. A. Chattopadhyay and A. J. Millis, *Phys. Rev. B* **64**, 024424 (2001).
14. K. Phillips, A. Chattopadhyay and A.J. Millis, *Phys. Rev. B* **67**, 125119 (2003).
15. M. Hamada and H. Shimahara, *Phys. Rev. B* **51**, 3027 (1995).
16. D. F. Agterberg and S. Yunoki, *Phys. Rev. B* **62**, 13816 (2000).
17. J. L. Alonso *et al.*, *Phys. Rev. B* **64**, 054408 (2001).
18. K. Pradhan and P. Majumdar, *Europhys. Lett.* **85**, 37007 (2009).
19. P. Sanyal and P. Majumdar, *Phys. Rev. B* **80**, 054411 (2009).
20. P. Sanyal, H. Das and T. Saha-Dasgupta, *Phys. Rev. B* **80**, 224412 (2009).
21. S. Kumar and P. Majumdar, *Eur. Phys. J. B* **50**, 571 (2006).
22. P. Fazekas, *Lecture Notes on Electron Correlation and Magnetism* (World Scientific, 1999), Chap. 4.5.
23. S. Jana *et al.*, *Phys. Rev. B* **86**, 054433 (2012).
24. J. Navarro *et al.*, *Phys. Rev. B* **64**, 092411 (2001).
25. B.-G. Park *et al.*, *Phys. Rev. B* **79**, 035105 (2009).
26. V. Singh and P. Majumdar, *Eur. Phys. J. B* **83**, 147 (2011).
27. C. R. Wiebe *et al.*, *Phys. Rev. B* **65**, 144413 (2002).

28. Aharen *et al.*, *Phys. Rev. B* **81**, 064436 (2010).
29. Aharen *et al.*, *Phys. Rev. B* **80**, 134423 (2009).
30. Asymptote: The vector graphics language, available at http://asymptote.sourceforge.net/.